Analysis of Area Spectral & Energy Efficiency in a CoMP-Enabled User-Centric Cloud RAN

Shahrukh Khan Kasi, *Student Member, IEEE,* Umair Sajid Hashmi, *Member, IEEE*, Muhammad Nabeel, Sabit Ekin, *Member, IEEE,* and Ali Imran, *Senior Member, IEEE*

***Abstract*—In this paper, we consider coordinated multipoint transmission (CoMP) by using distributed data base stations (DBSs) in a User-centric Cloud-based Radio Access Network (UCRAN). The creation of non-overlapping virtual cells (or service zones) centered around a user, contrary to traditional cellular architecture, shifts the mode of operation from base station centric "always ON" cells to user-centric "on-demand cells". In contrast to existing literature, we show that CoMP is only beneficial in network architectures where cell-edge users are present. In a UCRAN architecture, where the cell-edge users are virtually removed due to non-overlapping user-centric cells, the performance gain provided by enabling CoMP is insignificant. We analyze this by performing a comparative performance analysis of UCRAN with different joint transmission schemes of CoMP. We also provide analytical expressions for network-wide coverage probability, area spectral efficiency, and energy efficiency by taking advantage of the stochastic geometry tools. Additionally, we investigate the impact of new degrees of freedom such as the size of the service zones and density of data base station on the spectral and energy efficiencies of CoMP-enabled UCRAN. Extensive Monte Carlo simulations validate the proposed analytical framework as well as provide useful insights into the design of next-generation cellular architectures.**

***Index Terms*—CoMP, cloud radio access networks, user-centric networks, area spectral efficiency, energy efficiency.**

I. Introduction

THE large-scale permeation of mobile and Internet of Things (IoT) devices in every field of life have brought many challenges to the existing wireless network technologies. Unprecedented coverage and system capacity requirements demand a speedy resolution to challenges faced by the current wireless network technologies. The most viable solution is to enable heterogeneous networks (HetNets) technology instead of a homogeneous network to provide network densification [1]. HetNets, while capable of providing network densification, also aggravate the inter-cell interference in the network. Moreover, HetNets also increase the network operator's cost of operations owing to small cell's dense deployment [2], [3].

UCRAN has emerged as a promising technology to cope with the challenges introduced by HetNets. UCRAN enables the formation of virtual cells around scheduled users and consequentially removes the impact of dominant interferers, thus, alleviating the problem of inter-cell interference to a good extent. Architecturally, UCRAN dissociates the baseband processing unit from the radio access network allowing the dense deployment of data base stations (DBSs) without incurring high capital and operational cost because of the low-cost hardware requirements of radio access units. Furthermore, DBSs dense deployment reduces the average distance of user and serving base station which relaxes the transmission power requirement of both User Equipment's (UE) and DBSs [4].

From the architectural point of view, UCRAN enables dynamic coverage and offers a higher quality of experience (QoE) at the UE through spatial diversity [5]. For this reason, UCRAN is considered as an ideal architecture to support coordinated multi-point (CoMP) technology [6]. Using co-operative communications, CoMP solutions enhance the key performance indicators (KPIs) such as coverage probability, signal-to-interference ratio (SIR), and area spectral efficiency of a wireless network, however, at the expense of reduced energy efficiency [6].

While the primary motive behind CoMP is to improve the performance of cell-edge UEs [7], UCRAN can potentially remove cell-edge users by shifting the design of cellular network from base station centric to user centric [7]–[9]. Due to these contrasting properties, we hypothesize that CoMP may only be beneficial in network architectures where cell-edge UEs are present in the network. In the architecture envisaged for a UCRAN (details discussed in Section I-B), cell-edge UEs do not exist because of non-overlapping service zones created around scheduled UEs such that each UE is offered service only by the base station(s) in its respective service zone using spatial diversity techniques. Thus, the very purpose of CoMP to alleviate the cell-edge UEs is defeated which may result in the performance degradation of KPIs if CoMP is enabled in such a UCRAN architecture.

In this paper, we first extend the user-centric architecture proposed in our previous work [10] to a CoMP-based scenario. Then, using stochastic geometry concepts, we provide analytical expressions of coverage probability, area spectral efficiency, and energy efficiency in a CoMP-enabled UCRAN architecture. We discuss theoretical and simulation results on joint maximization of area spectral efficiency, and energy efficiency with the new degrees of freedom offered by the UCRAN architecture, such as the size of the virtual cluster (which we refer to as service-zone or S-zone). We further discuss network scenarios where CoMP-based deployment will benefit the overall network KPIs. Specifically, this paper aims to provide useful insights on the design and planning of future UCRAN networks by discussing the interplay of network parameters with system-level efficiency parameters.

Shahrukh Khan Kasi, Muhammad Nabeel, and Ali Imran are with the AI4Networks Research Center, School of Electrical & Computer Engineering, University of Oklahoma, OK, USA.

Umair Sajid Hashmi is with the School of Electrical Engineering & Computer Science, National University of Sciences & Technology, PK.

Sabit Ekin is with the Department of Electrical & Computer Engineering, Oklahoma State University, USA.

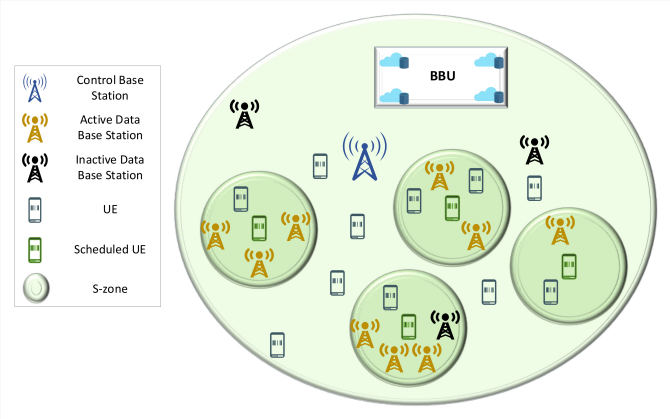

Fig. 1: CoMP-enabled UCRAN architecture with activation region of radius R_{szone} for a scheduled UE.

The work will pave way for employing artificial intelligence (AI) assisted self-organizing framework to dynamically adjust the network parameters such as S-zone size, DBS deployment density, and DBS power control strategies to jointly optimize the area spectral efficiency, energy efficiency, and other desired KPIs.

A. UCRAN Architectural Overview

UCRAN enables the provisioning of seamless coverage to UEs and provides demand-based baseband processing to radio remote heads or DBSs. The pool of baseband processing units (BBUs) collocated with the control base station (CBS) is responsible for turning DBSs ON/OFF given the service requirements of a scheduled UE. DBSs connectivity to a pool of BBUs is ensured via a fronthaul network comprising of optical fiber. In UCRAN, most of the signal processing is carried at a BBU while DBSs are used to provide coverage to a scheduled UE with minimal signal processing overhead [11].

The density of DBS deployment in future wireless networks is envisioned to be very high allowing UCRAN to substantially improve energy consumption by activating selective DBSs on-demand in S-zones contrary to always turned ON DBSs. Further, the size of the S-zone (virtual user-centric cell) operates as a proxy ensuring sufficient minimal separation between a scheduled UE and its nearest interfering DBSs thus eliminating cell-edge interference. Irrespective of a user's location and mobility, these non-overlapping S-zones can provide a seamless service experience to the UE utilizing the spatial diversity of DBSs.

Spatial diversity is considered one of the most popular techniques to improve communication reliability in different wireless networks [12]. In a UCRAN architecture, it is employed by dynamically selecting the best DBS(s) (in terms of channel gain) within an S-zone of a pre-defined radius around a UE. The UEs are scheduled at each transmission time interval (TTI) by the macro-cell or BBU according to their scheduling priorities. A predefined number of DBSs in an S-zone are activated at each TTI while the other DBSs are kept OFF to minimize interference. In every TTI, each scheduled UE is served by a maximum of M DBSs that provide the maximum channel gain in an S-zone. Fig. 1 provides a visual illustration of a UCRAN where the maximum number of cooperative DBSs is set to 3. In an S-zone with less than or equal to 3 DBSs, all the available DBSs are activated for cooperation. In an S-zone with more than 3 DBSs, only 3 DBSs that provide the maximum channel gain are activated for cooperation.

B. Related Work

CoMP solutions have been investigated for over two decades now, however, its incorporation in UCRAN based architecture is still in its fancy. In [13], the authors derived analytical expression based on two approximations for coverage probability in the downlink HetNet with user-centric architecture and base station cooperation. The numerical results, though highly accurate, lack a closed-form expression for the coverage probability. The authors have mainly focused on the analytical model for coverage probability and did not analyze the impact of cooperation on different KPIs in a user-centric network.

The authors in [14] formulated max-min rate problem to reduce the power consumption of UCRAN by joint optimization of beamforming weights and UE association with the access point. The formulated problem is first divided into two subproblems by relaxing the energy efficiency subproblem and power consumption subproblem and then solved separately utilizing the Lagrange duality method. Authors in [15] considered transmission points cluster approaches in massive multiple-input-multiple-output and millimeter-wave aided CRANs to reduce the overhead cost and ensure minimum signal changes at both network and user ends. In [9], the authors have derived approximate analytical expressions for the ergodic capacity and coverage probability for millimeter-wave user-centric dense networks.

In [16], the authors integrate CoMP and the non-orthogonal multiple access in downlink heterogeneous CRANs. Depending on the correlation of received signal power and dominant interferer signal power, they categorize users as CoMP or NoN-CoMP. The authors derive an analytical expression for achievable throughput using the tools of stochastic geometry. The authors in [17] provide a tractable analytical expression for spectral and energy efficiency in a traditional HetNet using the tools of stochastic geometry. The authors also provide analysis on optimizing spectral and energy efficiency given the transmit power and density of base stations.

In contrast to those previously reported in the literature, our study examines the average aggregate interference, the area spectral efficiency, and energy efficiency in UCRANs with CoMP. We derive closed-form expressions for the mentioned KPIs and provide a close bound to numerical results. The analysis is also extended for the different schemes of the joint transmission mode of CoMP (discussed in Section II-B). The obtained analytical and numerical model is then used to calculate the optimal S-zone size, DBS density, and other system parameters in terms of area spectral efficiency, and energy efficiency. To the best of the authors' knowledge, this work is a first attempt to quantify the impact of enabling CoMP in a UCRAN with non-overlapping S-zones.

C. Contributions

The contributions of this work can be summarized as follows:

- First, we extend the user-centric architecture proposed in [10] to include cooperation between DBSs in an S-zone. We characterize the activated DBS density followed by the average interference experienced by a scheduled UE in UCRAN using the stochastic geometry tools. (Section IV-A).
- In contrast to previous works, we derive a closed-form expression characterizing the lower bound on the probability of coverage for a scheduled UE in a CoMP enabled UCRAN (Section IV - B). The lower bound is further utilized to derive the area spectral efficiency in UCRAN (Section IV - C).
- We then proceed to quantify the energy consumption model for UCRAN to support CoMP communication and the associated overhead for discovering DBS(s) providing the highest channel gains at each scheduled UE. The power consumption model is used to derive the energy efficiency of CoMP-enabled UCRAN (Section V).
- Next, we provide a comparative performance analysis of different realizations of the joint transmission mode of CoMP in UCRANs. The three realizations are categorized based on the selection methods of cooperative DBSs in an S-zone (Section VI - C).
- Finally, the derived analytical framework is used to investigate the impact of new degrees of freedom, i.e., the S-zone size and DBS density, on the area spectral efficiency, and energy efficiency of CoMP-enabled UCRAN. The results indicate that for any number of cooperative DBSs in an S-zone, an optimal operating point for the S-zone size and density of DBS exists that maximizes the area spectral efficiency and energy efficiency. However, the S-zone size optimal for area spectral efficiency does not need to also be optimal for energy efficiency, therefore, we provide an analysis on the tradeoff of these KPIs using the new degrees of freedom (Section VI - D/E).

D. Paper Organization and Notation

Throughout this paper, the boldface small case letter (such as $\mathbf{x}$) is used to represent a vector, and $||\mathbf{x}||$ is used to denote the $L2$ norm of vector $\mathbf{x}$ in Euclidean space. The symbol / denotes the set subtraction, whereas $\in$ denotes the set membership. The notations $\mathbb{E}_Z(.)$ and $f_Z(.)$ are used to denote the average value and probability distribution of a random variable, respectively. The symbol $Z \sim U(a,b)$ indicates a uniform distribution for values between a and b. The symbol $Z \sim \exp(\mu)$ represents an exponential distribution with average value μ. The symbol $\mathbb{1}(x > y)$ denotes an characteristic function and $b(x,r)$ represents a circle centered at a point x with the radius of size r. Finally, the Poisson point process (PPP) is denoted by Π.

The rest of the paper is organized as follows. The problem description and research challenges are discussed in Section II. The network model is explained in Section III. The quantification of area spectral efficiency and energy efficiency are derived in Sections IV and V, respectively. System evaluation is conducted in Section VI. Finally, the outcomes of the paper are concluded in Section VII.

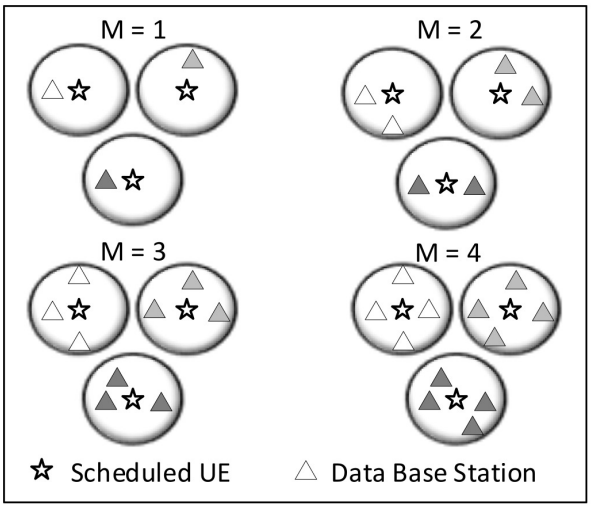

Fig. 2: Graphical realization of CoMP for different values of M where the different colors of DBSs correspond to DBSs of different S-zones.

II. Problem Description and Design Issues

In this Section, we first discuss the CoMP-enabled UCRAN architecture in detail. We then identify the key challenges in CoMP-enabled UCRAN architecture followed by the discussion of various methods through which CoMP can be employed.

A. CoMP-enabled UCRAN Architecture

In a UCRAN model, the S-zone of a predefined radius is created around all scheduled UEs during each TTI. An arbitrary UE is scheduled depending on its service requirements which is then served by one or more activated DBSs within an S-zone. The set of serving DBSs around a scheduled UE may change across TTIs depending on the spatial distribution of DBSs, user's mobility, and wireless channel conditions. If more than one DBS is activated, then a mechanism for cooperation is required to simultaneously transmit data to the scheduled user.

For LTE-advanced, 3GPP has identified three major downlink coordination techniques based on the complexities of implementation and required backhaul capacity [18]. These techniques can be categorized as (1) joint transmission (JT), (2) dynamic point selection (DPS), and (3) coordinated beamforming/scheduling (CB/CS). In JT, channel state information (CSI) and user data are shared between the coordinated set of transmission points. The mode of operations of DPS is very similar to JT except that the data is transmitted by one transmission point at a specific TTI. Unlike JT and DPS, CB/CS requires only CSI to be shared between the transmission points. Even though the backhaul bandwidth requirement of JT is the highest amongst all the aforementioned coordination techniques, the maximum gain in performance is also offered by JT [6].

In this work, we mainly focus on the realization of JT for enabling cooperation between the transmitting DBSs in an S-zone. To make a comparative analysis, we consider that at

any specific TTI, the number of cooperative DBSs in an S-zone cannot exceed $M \in Z^+$, where Z^+ is the set of positive integers. An exact bound on the number of cooperative DBSs is not considered because the number of DBSs in an S-zone depends on the density of DBSs, therefore, it is not realistic to assume that each S-zone will have at least a certain number of DBSs. In Fig. 2, we show the graphical realization of CoMP enabled UCRAN for different values of M. An important point to consider here is that in each S-zone, no more than M DBSs coordinate to simultaneously transmit the same data to the scheduled UE. Also, if the number of DBSs is less than M in any S-zone then all of them will be activated by the BBU to serve a scheduled UE (as shown in Fig. 2 for $M = 4$ scenario).

B. CoMP Clustering Challenges in UCRAN

CoMP is often realized with small clusters of DBSs due to the complexity required for coordination which increases exponentially with the increase in coordinated cells in a cluster [6]. An innate question that arises is whether the benefits of CoMP exceed the complexities involved in enabling it in a UCRAN. Although CoMP has been widely studied in HetNets, there has been limited work on CoMP in UCRAN. Therefore, we discuss the challenges faced by enabling CoMP in UCRAN which can be classified as:

Is it spectral-efficient and energy-efficient to realize CoMP? As briefly discussed in Section I (A), gains through enabling CoMP are achieved at the expense of energy efficiency. However, the underlying assumption that realizing CoMP increases the area spectral efficiency in any network may be too much of an exaggeration. The two important points to notice in the UCRAN architecture shown in Fig. 1 are that: (i) there are no cell-edge users because virtual cells are created around the users, and (ii) increasing coordinating DBSs in an S-zone leads to more number of activated DBSs in the overall network increasing the number of interferers in the network. By enabling CoMP, the dominant interferers are virtually removed which intuitively should reduce the overall interference experienced by a UE. However, in an architecture such as shown in Fig. 1 where S-zones are non-overlapping and DBSs are activated "on-demand" of a UE within a specific user-centric cell area (S-zone), the existence of dominant interferers is unfounded. Both of these observations are directly related to the spectral gains achieved by realizing CoMP because: (i) the major feature of CoMP, which is to mitigate cell-edge user interference, is not applicable in UCRAN architecture with non-overlapping S-zones, and (ii) interference is minimum only when one DBS is activated in every S-zone. However, ideal CoMP gains can only be achieved if the increase in received signal powers at the scheduled UEs through coordination is much more than the increase in the aggregate interference in the network.

It must be noted that by enabling CoMP, the number of coordinating DBSs increases but so does the number of interferers because more DBSs are activated in other S-zones. In the UCRAN architecture discussed in this work, the selection combining diversity technique is used to activate no more than M DBSs that provide the highest channel gains to a scheduled UE in an S-zone. Because of this reason, even if the number of coordinating DBSs is increased, the dominant impact on received signal power at a scheduled UE (in most cases) will be from the DBS providing the largest channel gain. The disparity in the channel gains from coordinating DBSs increases for higher values of the path-loss exponent. Contrarily, the increase in the number of interferers due to an increase in the number of activated DBSs will increase the overall interference experienced at a scheduled UE. This phenomenon increases the interference roughly by M fold while received signal power is not increased by the same factor leading to a decrease in SIR due to uncoordinated interference out of the S-zone. Based on the discussion, it is quite evident that whether CoMP transmission in UCRAN architecture will enhance spectral and energy efficiency is not a trivial research problem.

What is the optimal S-zone size? Another key parameter involved in the design of UCRAN is the size of the cooperative cluster or S-zone created around a scheduled UE. Increasing the S-zone size causes: (i) an increase in the average distance between scheduled UE and interfering DBSs, (ii) an increase in the possible set of DBSs within a cooperative cluster yielding high macro-diversity gain, and (iii) a possible decrease in the total number of activated DBSs because the number of activated DBSs in an S-zone is bounded by M in the UCRAN architecture shown in Fig. 1; meaning that if the total number of S-zones are decreased in a network, then the total number of activated DBSs will also decrease. Hence, larger the S-zone size, lesser the number of scheduled UEs and consequently activated DBSs serving those scheduled UEs. Conversely, larger S-zone sizes may lead to a decrease in the overall DBSs power consumption and increase spectrum reuse such that more number of scheduled UEs can be served simultaneously. Given these insights, we investigate the optimal S-zone size that yields an ideal tradeoff between area spectral efficiency, energy efficiency, or some combination of both in a CoMP-enabled UCRAN.

Which DBSs to activate/deactivate? Another important design parameter is to decide which DBSs should be kept activated and which DBSs should remain deactivated assuming that measurements of average received signal powers from all DBSs are available at a scheduled UE. In [7], the authors have discussed two schemes by which DBSs in JT can be activated/deactivated. In scheme 1, M DBSs that provide the best average received powers are activated while others are kept deactivated. In scheme 2, a cooperative DBS is only considered for CoMP if the received signal power from the DBS is above some percentage of the maximum received signal power. For example, if the maximum received signal power from all DBSs is P_{max}, then the received signal power from the cooperative DBSs P_{CoMP} should be greater than $\beta \times P_{max}$, where β can be any value between 0 and 1. Another method by which DBSs are activated/deactivated, termed as a random scheme, is to randomly activate DBS(s) in the S-zone while deactivating other DBSs. Therefore, DBSs activation/deactivation and its impact on area spectral efficiency, and energy efficiency in a CoMP enabled UCRAN architecture is an interesting research problem that we investigate in this work.

III. Network Model

A. Spatial and Channel Model

In this work, we consider an underlaid cloud radio access network with an ultra-dense DBS deployment scenario. The ultra-dense deployment of DBSs is an imaginable scenario in future networks [19]. Both DBSs and UEs are spatially modeled as independent stationary Poisson point processes Π_{DBS} and Π_{UE} with densities λ_{DBS} and λ_{UE}, respectively. The average number of DBSs in an S-zone is given by $\lambda_{DBS}\pi R_{szone}^2$ that is characterized by λ_{DBS} and Lebesgue measure [20] of a disc with radius R_{szone}.

The communication channel between an arbitrary user $x \in \Pi_{UE}$ and DBS $y \in \Pi_{DBS}$ is modeled by $h_{xy}\ell||x-y||$, where $h_{xy} \sim \exp(1)$ is a exponential random variable with unit mean representing the effects of Rayleigh fading and $\ell||x-y||$ is the large-scale path loss model. The large-scale path loss model is given by the frequency-dependent constant K, distance between the UE and DBS $||x-y||$, and path loss exponent $\alpha > 2$ such that $\ell||x-y|| = ||x-y||^{-\alpha}$. All DBSs are assumed to transmit at equal power levels P_{DBS}, and each DBS and UE is equipped with a single antenna. We also assume that the thermal noise is negligible, hence, the communication is interference-limited.

B. User-centric Clustering in UCRAN

In this work, we use the user-centering cluster mechanism given in Algorithm 1 [10] for UCRAN. The UEs are scheduled at each TTI by the macro-cell or BBU according to their scheduling priorities which are marked according to a uniform random distribution $p_{UE} \sim U(0,1)$. The lower the mark value of a UE, the higher the scheduling priority it possesses. For the UEs which are not scheduled yet, their scheduling priorities increase in the subsequent TTIs until they are scheduled to be served.

A UE x is scheduled (i.e., $p_{sch}^x = 1$) iff its scheduling priority is the highest in its neighborhood which is characterized by the cluster radius R_{szone}. To be succinct, this means that within a circle of radius R_{szone} centered at UE, there is no other UE with a higher scheduling priority, and the minimum distance between any two S-zones should be at least $2R_{szone}$. Note that this circle (S-zone) is commensurate to the size of the cooperative cluster. The dynamic change in S-zone size allows the flexibility to activate DBSs in an S-zone depending on which scheme of joint transmission is used to service a scheduled UE. A macro-cell or BBU is responsible for both the activation of DBSs in a cooperative cluster and delegating the size of a cooperative cluster to scheduled UEs.

The on-demand activation of DBSs makes UCRAN capable of self-organizing its coverage according to the spatiotemporal variation in the user demography. Though, for the UCRAN architecture to avoid coverage holes in areas where there are no DBSs available to provide coverage to a scheduled UE, DBSs need to be deployed densely so that at any time there is at least 1 DBS available to provide services to a scheduled UE. In the case of a void cluster, which is an unlikely scenario, the scheduled UE can be clustered together to nearby scheduled UEs using clustering strategies discussed in [21].

Algorithm 1 User Equipment Scheduling Algorithm in CoMP-based UCRAN

Input: $\Pi_{UE}, \Pi_{DBS}, R_{szone}$
Output: Π'_{UE}, Π'_{DBS}

Initialize the set of UEs and the activated DBS(s) as $\Pi'_{UE} \leftarrow \emptyset$, $\Pi'_{DBS} \leftarrow \emptyset$.
Assign random priorities to each UE based on $p_{UE} \sim U(0,1)$.
Update Π'_{UE} such that:
for $x \in \Pi_{UE}$ **do**
  $p_{sch}^x \leftarrow 1$
  for $y \in \Pi_{UE}$ **do**
    if $y \in b(x, 2R_{szone})$ and $p_{UE}(y) > p_{UE}(x)$ **then**
      if $y \neq x$ **then**
        $p_{sch}^x \leftarrow 0$
      else
        continue
    else
      continue
  if $p_{sch}^x == 1$ **then**
    $\Pi'_{UE} \cup x$
Update Π'_{DBS} such that:
for $m \in \Pi'_{UE}$ **do**
  $DBS \leftarrow \emptyset$
  for $n \in \Pi_{DBS}$ **do**
    if $n \in b(m, R_{szone}) \neq \Phi$ **then**
      $DBS \cup m$
  Rank DBS in order of smallest path-loss criteria such that path-loss (DBS_i) < path-loss (DBS_j), $\forall i < j$
  if $|DBS| \leq M$ **then**
    $\Pi'_{DBS} \cup DBS_i$, $\forall DBS_i \in DBS$
  else
    $\Pi'_{DBS} \cup DBS_i$, $DBS_i \in DBS$, $i \leq M$
Scheduled users Π'_{UE} are served from the coordinating DBSs Π'_{DBS}

C. Signal Model and Probe Cluster

Consider a scheduled UE $x \in \Pi'_{UE}$, where Π'_{UE} is the PPP representing scheduled UEs. Π'_{UE} unlike Π_{UE} is a non-stationary Poisson point process that can be modeled as a type II Matern hardcore process [20]. The density of scheduled UEs can be approximated by an equidistant stationary Poisson point process [22] given as:

$$\lambda'_{UE} = \frac{1 - \exp(-\lambda_{UE} 4\pi R_{szone}^2)}{4\pi R_{szone}^2}. \quad (1)$$

For a scheduled UE x, let $\Pi'^{C}_{DBS} = \Pi'_{DBS} \cap b(x, R_{szone})$ be the set of DBSs that are activated by the BBU to serve x based on a scheduling criterion [10]. Π'_{DBS} represents the spatial distribution of no more than M activated DBSs in an S-zone. Similarly, let $\Pi'^{I}_{DBS} = \Pi'_{DBS} \backslash \Pi'^{C}_{DBS}$ be the set of DBSs which are simultaneously transmitting to the scheduled UE $u \in Pi'_{UE}$ where $u \neq x$. Given these observations, we model

the received signal at a particular scheduled UE as:

$$q_x = \sum_{i \in \Pi'^{C}_{DBS}} \sqrt{P_{DBS} h_{ix} \ell ||x-i||} s_x + \sum_{u \in \Pi'_{UE} \setminus x} \sum_{j \in \Pi'^{I}_{DBS}} \sqrt{P_{DBS} h_{jx} \ell ||x-j||} s_u, \quad (2)$$

where s_x is the signal transmitted to a scheduled UE x. Capitalizing on the stationary characteristics of the scheduled UE's PPP, focusing on a typical UE is sufficient. As maintained by Silvnyak's theorem [20], the addition of a single point does not affect the law of stationary PPP, therefore, a probe UE is added at the origin. Additionally, the received signal q_x can be simplified with $\ell||i-y|| = ||i-y||^{-\alpha} = ||i-o||^{-\alpha}$ where the index o is the location of a typical UE.

IV. Characterizing the Area Spectral Efficiency of a UCRAN

A typical UE is served by at most M DBSs in an S-zone centered at origin o with a ball area of $b(o, R_{szone})$ where R_{szone} is the radius of the ball. The cooperative cluster is defined as:

$$C = arg_{r_1, r_2, ..., r_n \subset \Pi'_{DBS}} \sum_{i=1}^{n} h_i r_i^{-\alpha}, \quad (3)$$

where $n \leq M$, r_i denotes the distance between serving DBS i and scheduled UE, h_i captures the effect of Rayleigh fading, and Π'_{DBS} is the resultant PPP of activated DBS with density λ'_{DBS}. With the joint transmission mode of CoMP, all the DBSs in a cooperation set jointly transmit the same message to a scheduled UE on the same time-frequency resource [23], [24]. Therefore, the signal-to-interference ratio at a typical UE in an interference-limited environment can be expressed as:

$$SIR = \Gamma_{UE} = \frac{\sum_{i \in \Pi'^{C}_{DBS}} h_i r_i^{-\alpha}}{\sum_{j \in \Pi'^{I}_{DBS}} h_j r_j^{-\alpha}}. \quad (4)$$

The noise power at a scheduled UE is at much lower levels as compared to the aggregate interference which is why the assumption of an interference-limited environment is valid even with the induced spatial repulsion between scheduled UEs and activated DBSs in other S-zones [13].

A. Expected Aggregate Interference and Modified Density of Activated DBSs

According to reduced Palm measure and Slivnyak's theorem [20], the expected aggregate interference at a typical UE can be expressed as:

$$\mathbb{E}_{\mathbf{I}}[I] = \mathbb{E}\left(\sum_{j \in \Pi'^{I}_{DBS}} h_j r_j^{-\alpha} \right). \quad (5)$$

According to Campbell's theorem [20], the expectation term in above expression can be simplified to:

$$\mathbb{E}_{\mathbf{I}}[I] = \int_{R_{szone}}^{\infty} 2\pi \lambda'_{DBS} \mathbb{E}[H] r^{1-\alpha} dr, \quad (6)$$

where λ'_{DBS} is the density of activated DBSs and $\mathbb{E}[H]$ is the expected value of small-scale fading. By integrating and substituting $\mathbb{E}[H] = 1$, we get:

$$\mathbb{E}_{\mathbf{I}}[I] = \frac{2\pi \lambda'_{DBS}}{(\alpha - 2)(R_{szone}^{\alpha-2})}. \quad (7)$$

The density of activated DBSs λ'_{DBS} can be approximated as $p_{ACT} \lambda_{DBS}$, where λ_{DBS} is the density of original DBSs distribution and p_{ACT} is the activation probability of DBSs in an S-zone.

Theorem 1. The activation probability of DBSs in a CoMP-enabled UCRAN can be expressed as follows:

$$p_{ACT} = \left(1 - \exp(-\lambda'_{UE} \pi R_{szone}^2)\right) \cdot \left(\frac{\Gamma(M+1, X)}{\gamma(M+1)} + \exp(-X) \left[\frac{M(X)^{M+1} {}_2F_2(1, M+1; M+2, M+2; X)}{(M+1)\gamma(M+2)} - 1 \right] \right), \quad (8)$$

where ${}_pF_q(a_1, ..., a_p; b_1, ..., b_q; z)$ is the generalized hypergeometric function, $\gamma(x)$ is the complete gamma function, $\Gamma(x, y)$ is the upper incomplete gamma functions and $X = \lambda_{DBS} \pi R_{szone}^2$ is the average number of DBSs in a circle.

Proof: See Appendix A. ∎

From Eq. (7) and Eq.(8), we make the following remarks:

- Expected aggregate interference increases with the increase in the density of activated DBSs which is a function of M, R_{szone}, λ'_{UE} and λ_{DBS}. However, for a fixed density of scheduled UEs and DBSs, the only tunable parameters are M and R_{szone}. Both parameters will have a direct impact on the average aggregate interference experienced at a typical scheduled UE.
- It can be observed that by enabling CoMP, i.e., $M > 1$, the average aggregate interference will increase exponentially with the increase in M. Likewise, reducing the S-zone size will increase the overall number of DBSs activated for serving scheduled UEs, thereby leading to an increase in average aggregate interference.

B. Coverage Probability

A typical UE's probability of coverage can be defined as the probability of received SIR to be greater than a desired SIR threshold value (γ_{th}). The mathematical expression of the coverage probability can be simplified as:

$$P_{cov}(\gamma_{th}, R_{szone}) = P_r(\Gamma_{UE} \geq \gamma_{th}) = 1 - P_r(\Gamma_{UE} < \gamma_{th}). \quad (9)$$

Substituting the value of Γ_{UE} from Eq. (4) in Eq. (9), we obtain:

$$P_{cov}(\gamma_{th}, R_{szone}) = 1 - P_r\left(\frac{\sum_{i \in \Pi'^{C}_{DBS}} h_i r_i^{-\alpha}}{\sum_{j \in \Pi'^{I}_{DBS}} h_j r_j^{-\alpha}} < \gamma_{th} \right) = 1 - P_r\left(\sum_{i \in \Pi'^{C}_{DBS}} h_i r_i^{-\alpha} < \gamma_{th} \sum_{j \in \Pi'^{I}_{DBS}} h_j r_j^{-\alpha} \right). \quad (10)$$

Considering the aggregate interference in the above expression as a random variable, we can average the SIR distribution over all instances of interference between non-cooperating

active DBSs that will allow us to simplify the above expression as:

$$P_{cov}(\gamma_{th}, R_s zone) = 1 - \mathbb{E}_{\mathbf{I}}\Big[P_r\Big(S < \gamma_{th} I\Big)\Big], \quad (11)$$

where $S = \sum_{i \in \Pi'^{C}_{DBS}} h_i r_i^{-\alpha}$ and $I = \sum_{j \in \Pi'^{I}_{DBS}} h_j r_j^{-\alpha}$ denote the desired signal power and aggregated interference strength, respectively.

Theorem 2. The lower bound on the coverage probability of the typical user in a CoMP-enabled UCRAN can be given as follows:

$$P_{cov}(\gamma_{th}, R_{szone}) \geq 1 - \exp\left(-\frac{\lambda_{DBS}\pi^{1-\delta}\delta\gamma\left(\delta, \frac{\gamma_{th}2\pi\lambda'_{DBS}R^2_{szone}}{\alpha-2}\right)}{(\gamma_{th}2\lambda'_{DBS})^{\delta}(R_{szone})^{-\delta(\alpha-2)}(\alpha-2)^{-\delta}}\right), \quad (12)$$

where $\delta = \frac{2}{\alpha}$ and $\gamma(a,b) = \int_a^b t^{a-1}\exp(-t)dt$ is the lower incomplete Gamma function.

Proof: See Appendix B. ∎

C. Area Spectral Efficiency

Building on the coverage probability metric obtained, we define the area spectral efficiency (ASE) performance metric in this Section. The average area spectral efficiency can be defined as [25],

$$ASE = \lambda'_{UE}\log_2(e)\int_0^{\infty}\frac{P_{cov}(\gamma_{th}, R_{szone})}{1+\gamma_{th}}d\gamma_{th}, \quad (13)$$

where λ'_{UE} is the modified density of the PPP representing scheduled users. Under the assumption that all users transmit at the same rate $\log_2(1+\gamma_{th})$ and the transmission is considered successful only if the received SIR is above the desired threshold γ_{th}, the ASE metric can be lower bounded [26] as

$$ASE = \lambda'_{UE}\log_2(1+\gamma_{th})P_{cov}(\gamma_{th}, R_{szone}). \quad (14)$$

Given a desired threshold, the average area spectral efficiency metric represents the sum of the maximum of average bits transmitted per unit Hertz bandwidth per unit area. It is worth noting that ASE is dependent on the density of scheduled UEs, γ_{th} and coverage probability. The bound for coverage probability and density of scheduled UEs will be tight for any value of γ_{th}, however, the multiplication of term $\log_2(1+\gamma_{th})$ with coverage probability and density of scheduled UEs is expected to slightly loosen the bound of ASE values for higher values of γ_{th}.

Similar to the coverage probability, ASE is also coupled with the size of the S-zone and the density of activated DBSs. While an increase in the cluster size reduces the density of scheduled UEs, it also improves SIR due to a reduction in the number of interfering DBSs. Similarly, by enabling CoMP, an increase is expected in the received signal power at a typical UE. However, CoMP also increases the number of interfering DBSs. Therefore, both these parameters can be treated as the design parameters of a UCRAN architecture for which there exist optimal values which maximize the network-wide ASE.

V. Characterizing The Energy Efficiency Of A UCRAN

In this Section, we quantify the energy efficiency (EE) performance of the proposed CoMP-enabled UCRAN architecture. Enabling CoMP and exploiting spatial diversity gain by activating DBS(s) with maximum channel gains will increase the energy consumption cost. At the same time, only activating some DBSs will improve the energy efficiency compared to the mechanism in which all the DBSs are kept ON [27], [28]. The energy efficiency can be formulated as [29]:

$$EE = \frac{\log_2(1+\Gamma_{cran})}{P_{cran}}, \quad (15)$$

where P_{cran} is the average power consumption of the whole network and Γ_{cran} is the effective SIR [29]. In the power consumption model, we focus on the overhead associated with enabling CoMP and discovering the best DBS(s) for the scheduled user association. During the discovery process, each DBS estimates the channel gain from the scheduled UE which will contribute to the energy consumption of the network.

The power consumption model proposed in this work is inspired from [30], wherein the authors proposed an accurate model for power dissipation considering parameters such as cooling, power amplifiers, baseband processing, and antenna interface. A related but modified model designed specifically for C-RAN was provided in [31] that uses parameterization specific to C-RAN efficiency.

The average power consumption can be modeled as:

$$P_{cran} = \omega_{cran}(N,\theta)P_O + P_{sp} + \Delta_u P_u + P_{ou}, \quad (16)$$

where P_O is the power consumption of the DBS allowing it to operate in listening mode, P_u is the transmission power of a UE, Δ_u is a factor for radio frequency module of power consumption at the UE, P_{ou} is the circuit power consumed at the UE, and P_{sp} is the power consumption due to signal processing overhead. The UCRAN coefficient is directly proportional to the average number of cooperative DBSs in each S-zone (represented by N) and a parameter θ which characterizes the implementation efficiency. By using a simple linear parameterization, the UCRAN coefficient can be modeled as $\omega_{cran}(N,\theta) = \theta N$ where $0 \leq \theta \leq 1$. In this work, θ is set to 1 to realize the least efficient UCRAN implementation in terms of fixed power consumption of activated DBSs.

Further, enabling CoMP requires additional power consumption for signal processing. The signal processing overhead required for CoMP is calculated as [32],

$$P_{sp} = 58(0.87 + 0.03N^2), \quad (17)$$

where N is the average number of cooperative DBSs activated in each S-zone and is given by $N = \lambda'_{DBS}/\lambda'_{UE}$. The network power consumption can now be given as:

$$P_{cran} = NP_O + 58(0.87 + 0.03N^2) + \Delta_u P_u + P_{ou}. \quad (18)$$

From the expression given in Eq. (15), it can be observed that EE is a function of the size of the S-zone, density of activated DBSs, and the number of cooperating DBSs. However, the optimal values of these parameters will be different for ASE and EE leading to an important design question as to

TABLE I: Simulation Parameters.

Symbol	Parameter Name	Parameter Value
-	Dimensions of Simulation Region	$100\,m \times 100\,m$
λ_{UE}	UE's average density	$10^{-1}\backslash m^2$
λ_{DBS}	DBS's average density	$3 \times 10^{-2} - 1.3 \times 10^{-1}\backslash m^2$ (Variable)
$\alpha, \alpha_{near}, \alpha_{far}$	Path-loss exponents	$3, 3, 6$
R_{szone}	S-zone Size	$1\,m - 10\,m$ (Variable)
M	Maximum Number of Cooperative DBSs	$1 - 5$ (Variable)

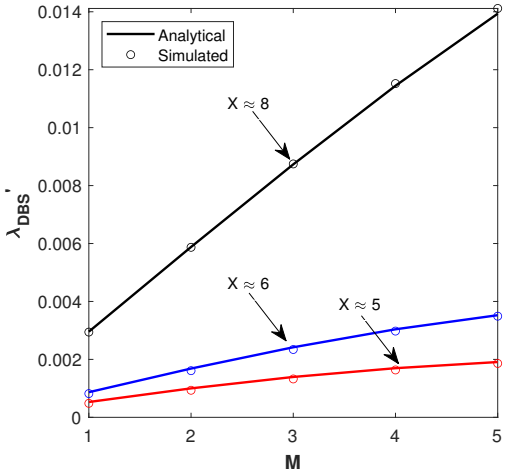

Fig. 3: Average activated DBS density (λ'_{DBS}) in the network for different numbers of maximum cooperating DBSs (M) within an S-Zone.

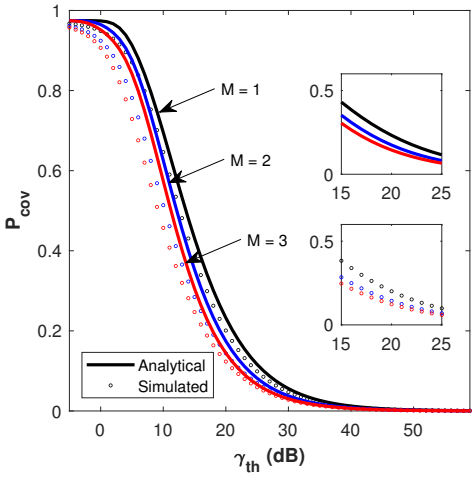

Fig. 4: Coverage probability for different SIR requirements (γ_{th}) and numbers of maximum cooperating DBSs (M) within an S-Zone for joint transmission scheme 1.

what values should be chosen to maintain a balance between the system's area spectral efficiency, and energy efficiency. In the next Section, we discuss the system evaluation considering the above-mentioned design question.

VI. System Evaluation

In this Section, we evaluate the performance of the proposed CoMP-enabled UCRAN using MATLAB simulations by setting the simulation parameters as shown in Table I. The service area under consideration is a square of 100 $m \times 100$ m. In the service area, UEs and DBSs are distributed through Poisson point processes with densities λ_{UE} and λ_{DBS}, respectively. At each TTI, UEs are scheduled according to the algorithm initially proposed in [10] and discussed in Section III. The size of the virtual cell (S-zone) and density of DBSs are varied across different experiments to study their impact on ASE and EE of a CoMP-enabled UCRAN. The transmission power value of each activated DBS is set to 1 Watt and the path-loss exponent is set to 3. The maximum size of cooperative DBSs is set to M and Monte-Carlo simulations are employed for 10^4 realizations in each experiment.

A. Validation of the Modified Density of DBSs

Fig. 3 presents the validation of the analytical model for the modified density of DBSs expressed in Eq. (8). For different values of M, the theoretical values are consistent with the simulated values of DBSs modified density. As expected, the density of activated DBSs λ'_{DBS} increases with an increase in M due to more number of activated DBSs in each S-zone.

Similarly, the impact of average number of DBSs within a circular region (calculated as $X = \lambda_{DBS}\pi R^2_{szone}$) can be observed by varying the DBS deployment density (λ_{DBS}) and the radius of the S-zone (R_{szone}). For X approximately equal to 8, 6, and 5, the density of activated DBSs decreases as the value of X is decreased. This is mainly because X is the average number of DBSs in a circle that can vary across different S-zones depending on the random distribution of the Poisson point process. However, if $M << X$ then for different values of X, there will be little or no impact on the density of activated DBSs as each S-zone will probably have at least M DBSs.

B. Validation of Coverage Probability for JT scheme 1

Fig. 4 compares the analytical and simulated results of coverage probability with different values of desired SIR thresholds γ_{th} for both CoMP-enabled and no-CoMP scenarios. It can be observed that with the increase in the value of γ_{th}, coverage probability is decreased. Moreover, the analytical coverage probability curves provide a lower bound to the simulated curves (as discussed in Section IV).

It is also important to note that there is a slight offset in the analytical and simulated curves for different values of the maximum number of cooperative DBSs in an S-zone, i.e., M. This offset, also observed by authors in [33], can be explained by recalling the derivation of expected aggregate interference expression in Section IV. In the devised analytical model, the Campbell theorem assumes an infinite number of interferes in the network. However, in our simulations, we can only consider a finite service region consequentially resulting in a finite number of interferers. The difference in the analytical and simulated aggregate interference contributes to the offset

TABLE II: Power Consumption Parameters.

Symbol	Parameter Name	Parameter Value
P_u	UE transmit power	1 W
P_O	DBS fixed power consumption	6.8 W
Δ_u	Radio frequency component's power consumption	4 W
P_{ou}	UE device discovery circuit power consumption	4.3 W

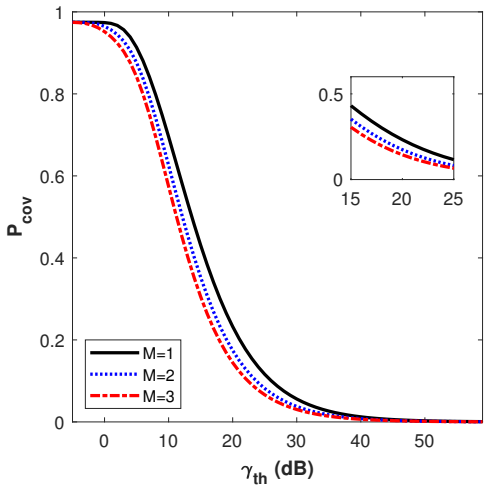

(a) Scheme 1.

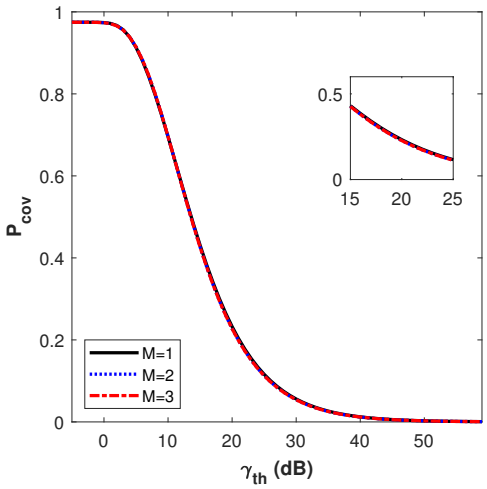

(b) Scheme 2.

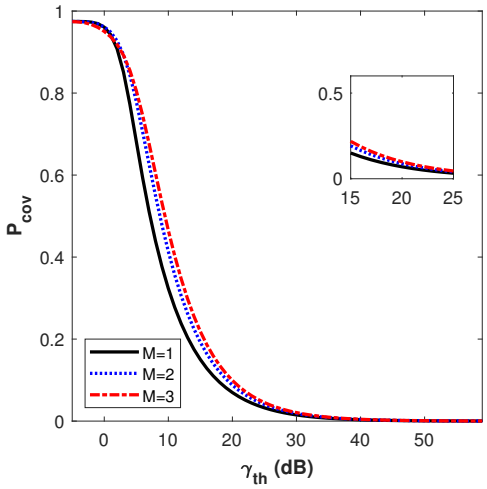

(c) Scheme 3.

Fig. 5: Performance comparison of coverage probabilities for scheme 1, scheme 2 and scheme 3 of joint transmission mode.

observed in the coverage probability curves.

Another interesting observation in Fig. 4 is the difference in the coverage probabilities of CoMP-enabled and no-CoMP UCRAN architectures. As discussed in Section II, the UCRAN architecture with non-overlapping S-zones removes the possibility of cell-edge UEs, therefore, the major feature of CoMP to alleviate cell-edge interference is not applicable. Without any cell-edge UE, the only constructive impact of CoMP is the increase in accumulated signal powers due to coordination in an S-zone. However, by activating DBSs according to scheme 1 of JT (spatial diversity technique), the DBS chosen first will always be a dominant contributor towards the accumulated signal power. Therefore, when CoMP is enabled, the signal powers will only increase by a small fraction due to the random deployment of DBSs and the path-loss model. On the other hand, the aggregate interference will increase linearly resulting in the degradation of coverage probability at a typical UE.

C. Comparison of JT Schemes Coverage Probability

In Section II, we discussed different schemes of joint transmission mode based on which DBSs are activated. In Fig. 5, we compare the performance of different schemes in terms of coverage probabilities. By employing scheme 2 of joint transmission, we only choose DBSs for cooperation if $P_{CoMP} > 0.9P_{max}$, where P_{CoMP} is the received signal power of cooperative DBS and P_{max} is the maximum of all

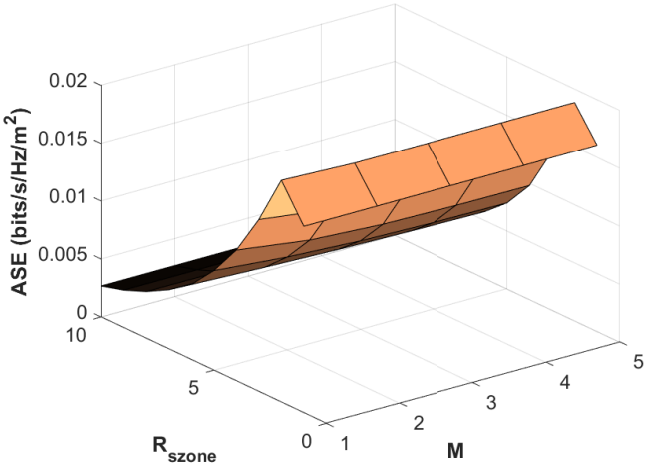

(a) $\lambda_{DBS} = 0.03$.

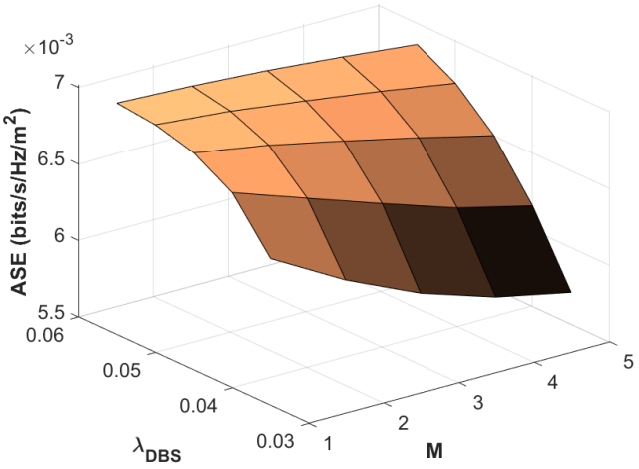

(b) $R_{szone} = 6\ m$.

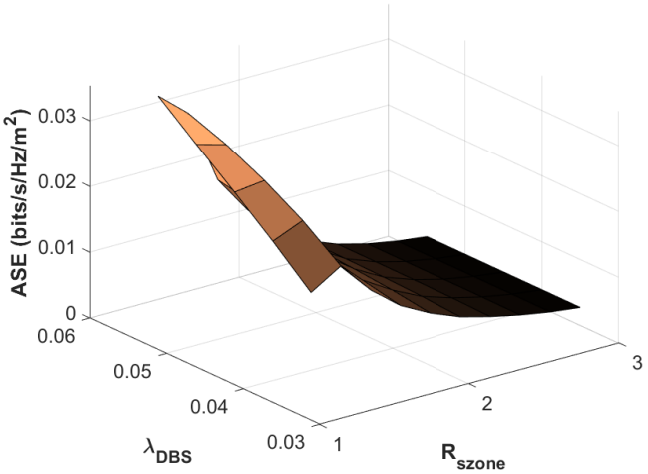

(c) $M = 2$

Fig. 6: Area spectral efficiency of the CoMP-enabled UCRAN with varying S-zone radius, DBS density and M for $\gamma_{th} = 4\ dB$.

received signal powers in an S-zone.

As discussed in the previous subsection that the dominant contributor in signal power is always the DBS that provides the maximum channel gain, therefore, occasionally, the signal power of the second maximum or third maximum DBS satisfies the criterion of scheme 2. For this reason, in Fig. 5 (b), it can be observed that the coverage probabilities for CoMP or no-CoMP are approximately the same. Enabling CoMP in UCRAN architecture using schemes 1 and 2 does not improve the coverage probabilities at an arbitrary UE. Hence, it buttresses our claim that enabling CoMP in UCRAN with the proposed architecture degrades the performance in terms of coverage probability, ASE, and EE (as further shown in Fig. 6 and 7). However, employing a random scheme of DBS selection where no more than M DBSs are randomly selected in each S-zone will show the improvement in terms of coverage probability in a CoMP-enabled UCRAN (as shown in Fig. 5 (c)). Nevertheless, the random selection of base stations is not a realistic scenario since in most cellular networks the base station offering the strongest channel link between UE and base station is selected for communication. Though for the test of concept, we show the results for the random scheme of JT in Fig. 5 (c).

JT with a random selection of DBSs is one such instance where employing CoMP in a UCRAN architecture with non-overlapping S-zones will not degrade the performance in terms of coverage probability. However, notice that the coverage probability for $M = 1$ in a random scheme is much less than the coverage probability for $M = 1$ in scheme 1 and scheme 2 because spatial diversity is not utilized in the random scheme.

From the results shown in Fig. 5, we can establish that the joint transmission technique of CoMP will not benefit the user-centric network, however with the requirement that: (i) the user-centric virtual clusters (S-zones) are non-overlapping, (ii) DBSs are activated using selection combining in an S-zone, and (iii) the communication path between scheduled UE and activated DBSs are not blocked by blockages. If any of the three conditions are not met, then the one-to-one link between

the transmission technique of CoMP and its benefits in a user-centric scenario cannot be established.

D. Optimal S-zone Radius and DBS Density for ASE

In Fig. 6 (a), the area spectral efficiency is plotted for different values of S-zone radius and M. We anticipate the existence of an optimal S-zone size at which the network-wide ASE is maximum. Further, the optimal S-zone radius to maximize ASE is expected to be smaller in magnitude as compared to S-zone size which maximizes EE. With the increase in the S-zone radius, the density of scheduled UEs reduces, thereby affecting the network ASE. Similarly, a decrease in the S-zone radius increases the density of scheduled UEs at the risk of spatially closer S-zones that increases interference levels. Therefore, as mentioned previously, the optimal S-zone radius should be a small value but not too negligible.

In Fig. 6 (a), we note that the optimal S-zone radius is 1.5 m which is slightly larger than the minimum considered S-zone radius of 1 m, hence, supporting our hypothesis. We also observe that the performance in terms of ASE is consistent across different M. This is mainly because ASE is dependent on the density of scheduled UEs, desired SIR threshold, and coverage probability. The desired SIR threshold does not change and the change in coverage probability is almost negligible when CoMP is employed. Therefore, the optimal S-zone size is not overly sensitive to the value of M unless the coverage probability change is significant between CoMP and no-CoMP scenarios.

In addition to S-zone radius, the density of DBSs that can maximize ASE is also an important design parameter from the perspective of a network operator. In Fig. 6 (b), the area spectral efficiency is plotted for different values of DBS density and M. From the figure, we can see that ASE increases monotonically with an increase in DBS deployment density for a fixed S-zone size. This is mainly because with larger DBS density, (i) the chances of coverage holes where no DBSs are available to provide service to a scheduled UE decrease, and (ii) there exist more options to activate the DBS(s) with strongest channel gains to further exploit spatial diversity. Also, for lower DBS density, employing CoMP significantly reduces the ASE, whereas, for higher DBS density, the performance in terms of ASE is consistent across different M.

Finally, the network ASE is plotted for different values of S-zone size and DBS density. For an optimal S-zone radius, ASE improves with the increase in the density of DBSs. Contrarily, given a fixed DBS density, ASE after an initial jump at $R_{szone} = 1.5\,m$ is decreased with the increase in S-zone radius. From these observations along with the observations reported in Fig. 6 (a) and (b), we can conclude that the radius of S-zone, DBS density, and the maximum number of cooperative DBSs greatly impact ASE. To maximize ASE, all of these inter-linked parameters should be jointly optimized through a self-organizing framework in future work.

E. Optimal S-zone Radius for EE

In Fig. 7, the energy efficiency is plotted for different values of S-zone radius and M. The power consumption parameters are summarized in Table II. Similar to ASE, the existence of an optimal S-zone size for which the EE will be maximum is obvious. However, the S-zone radius that will maximize EE is expected to be different than the S-zone radius that would maximize ASE. Intuitively, the S-zone radius that maximizes EE should be larger because by increasing the S-zone radius, the density of activated DBSs reduces resulting in lesser power consumption. From Fig. 7, we observe a similar trend where the EE is maximum for the largest S-zone radius. Also, for a fixed S-zone radius, enabling CoMP increases the power consumption of the network due to increased signal processing and additional power consumption overhead resulting in the degradation in EE of the system. Thus, we can easily conclude that EE degrades by enabling CoMP in UCRAN architecture with non-overlapping S-zones.

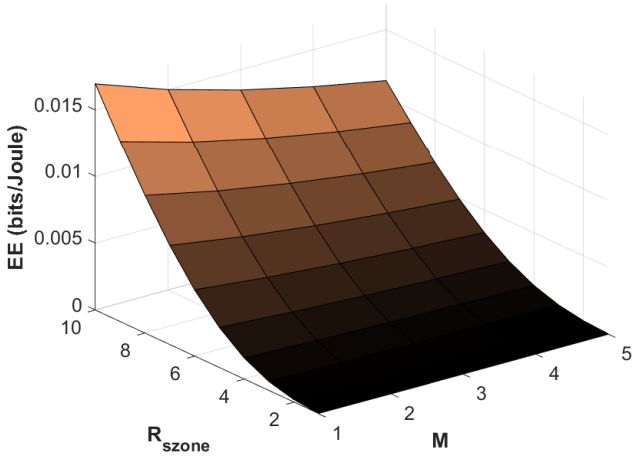

Fig. 7: Energy efficiency of the CoMP-enabled UCRAN with varying S-zone radius and M for $\gamma_{th} = 4\ dB$.

These results further second the need for an AI-assisted self-organizing framework that can capture the tradeoff of ASE and EE to jointly maximize both KPIs given the new degrees of freedom such as S-zone radius and density of DBSs. Also, the results support the hypothesis presented in Section I that employing CoMP will not only affect the system's energy efficiency but will also negatively impact the area spectral efficiency as well as coverage probability in UCRAN.

F. Performance Comparison for Mean Serviced UEs' ratio

Fig. 8 shows the comparison of the average number of UEs that are serviced out of the total scheduled UEs for varying values of S-zone radius, SIR desired threshold, and M. A UE is offered service iff: (i) there is at least 1 DBS present in the S-zone, and (ii) the average received SIR at the UE is greater than the desired SIR threshold. From the result shown in Fig. 8, a similar trend can be observed in the mean serviced UEs' ratio as observed in the coverage probability (scheme 1) with the enabling of CoMP. The decrease in the mean serviced UEs' ratio for $M > 1$ can be attributed to the increased interference in the network that affects the SIR received at a typical UE. We also observe that with an increase in SIR requirement threshold values (γ_{th}), the mean serviced UEs' ratio also decreases.

Additionally, the impact of R_{szone} on the mean scheduling UEs' ratio is demonstrated in Fig. 8. Intuitively, for a larger S-zone radius: (i) the inter-cell separation increases effectively reducing the interference at a typical UE, and (ii) the average

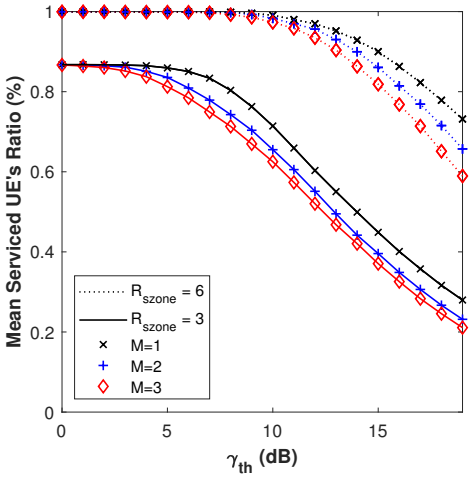

Fig. 8: UE servicing ratio comparison of proposed UCRAN approach.

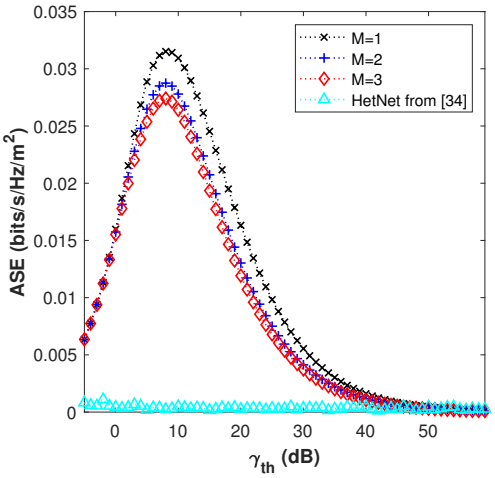

Fig. 9: ASE comparison of proposed UCRAN approach and traditional HetNet for different values SIR requirements.

number of DBSs available in an S-zone is increased effectively increasing the probability that there will be at least 1 DBS within the S-zone. For both of the above reasons, we observe a trend shown in Fig. 8 in which the mean service UEs' ratio increases when R_{szone} is increased from 3 to 6.

G. Performance Comparison with Traditional HetNet

Fig. 9 shows performance improvement in area spectral efficiency for the proposed CoMP-enabled UCRAN architecture (with S-zone radius = $2\,m$) in comparison to a traditional heterogeneous network architecture discussed in [34]. From the figure, we can observe that there is a massive increase (of the order of x100 and more) in the ASE of the proposed UCRAN approach as compared to the traditional HetNet. This is mainly because the traditional HetNet architecture can experience extreme inter-cell interference in a dense network due to its cell-centric architecture. To overcome inter-cell interference, the proposed UCRAN architecture not only provides a certain minimum separation between scheduled UEs but also provides dynamic coverage to each UE effectively resulting in higher ASE.

Another interesting observation from Fig. 9 is the existence of an optimal SIR threshold γ_{th} for which the ASE is maximized in CoMP-enabled UCRAN. The reason is more mathematical rather than conceptual and can be better explained by referring to the expression given in Eq. (14). For the same R_{szone} and user density, the density of scheduled UEs remains constant. The ASE thus changes with fluctuations in the SIR threshold or coverage probability. Now as the SIR threshold increases, two interactions are happening simultaneously which affect the ASE. First, with the increase in the SIR threshold, the term $\log_2(1+\gamma_{th})$ also increases resulting in increased ASE. Second, an increase in the SIR threshold, as observed in Fig. 4, reduces the coverage probability. Due to these contrasting effects, we observe a high jump in ASE values which then plummets as coverage probability approaches zero. The strong interplay of γ_{th} and coverage probability on ASE of the system will be further explored in future work.

H. CoMP-enabled UCRAN with Dynamic Blockages

After reviewing the simulation analysis hitherto, a reader may question the applicability of CoMP in user-centric networks where cell-edge users are diminished. Till now, we have shown that enabling CoMP for UEs that maintain a certain minimum repulsion with other UEs degrades the network performance in terms of important KPIs such as coverage probability, area spectral efficiency, and energy efficiency. However, there are many possible scenarios in which CoMP may be able to provide better reliability effectively enhancing the system's area spectral efficiency.

In this Section, we briefly discuss one such scenario where DBSs operate on high-frequency bands that are highly sensitive to blockages. We assume a simplified scenario in which the line of sight (LOS) link between DBSs and UEs is affected by the presence of blockages. The presence of blockages divides the network region into two parts, near-field, and far-field regions. The near-field and far-field regions can be best described by a dual-slope path loss model (DSPM) that have different path-loss exponents α_{near} and α_{far} for near-field and far-field, respectively, where $\alpha_{far} \geq \alpha_{near} > 2$ [35]. Note that higher values of α_{far} will result in sufficiently large path-loss, effectively causing the interference caused by DBSs beyond a critical distance (d_c) to approach zero. Also, we assume that a non-LOS link within an S-zone may not be able to provide sufficient signal strength to the UE, thus changing the state of the DBS-UE link to outage when affected by an obstacle. The standard dual path-loss model is given as [36]:

$$DSPM(x) = \begin{cases} ||x||^{-\alpha_{near}}; & \text{with } 1 - p_{blockage}(x) \\ d_c^{\alpha_{diff}} ||x||^{-\alpha_{far}}; & \text{with } p_{blockage}(x), \end{cases} \tag{19}$$

where $\alpha_{diff} = \alpha_{far} - \alpha_{near}$, $d_c > 0$ is the critical distance assumed to be equal to 1 meter and x is the distance (in meters) between the DBS and UE.

The blockage/non-LOS probability proposed by 3GPP is

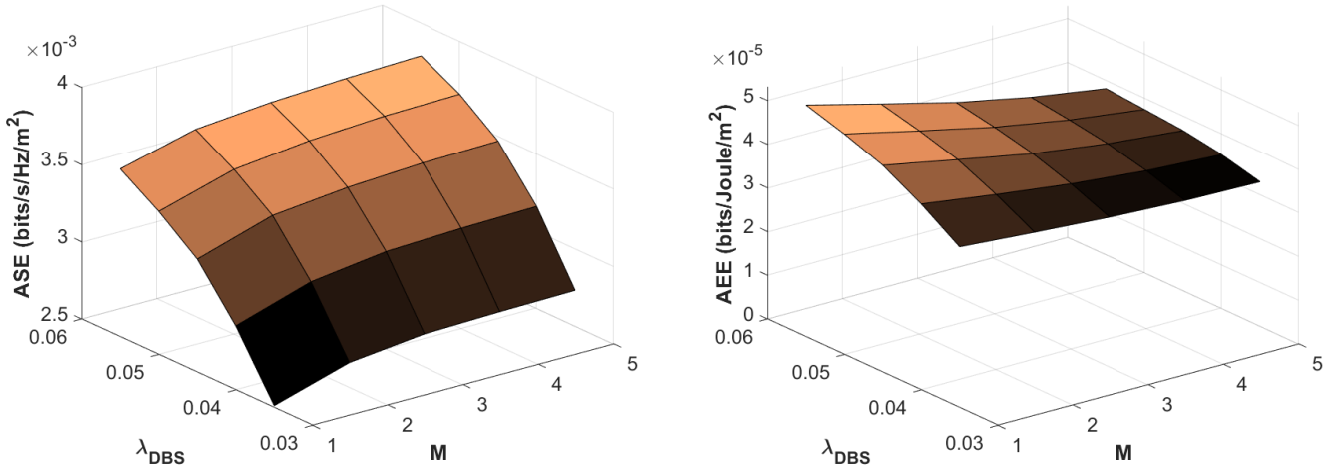

(a) Area spectral efficiency.

(b) Area energy efficiency.

Fig. 10: Performance comparison of CoMP-enabled UCRAN with dynamic blockages with varying DBS densities and M for $\gamma_{th} = 4\ dB$, $R_{szone} = 6m$, $\alpha_{near} = 3$ and $\alpha_{far} = 6$.

given as [37]:

$$p_{blockage}(x) = 1 - \left(0.5 - \min\left(0.5, 5\exp\left(-\frac{156}{x}\right) + \min\left(0.5, 5\exp\left(-\frac{x}{30}\right)\right)\right)\right). \quad (20)$$

We expect that due to random blockages, the communication between serving DBSs and UEs will be highly affected. In such a scenario, CoMP will be able to provide second-tier protection from service degradation due to blockages. In Fig. 10 (a), the area spectral efficiency is plotted for different values of DBS densities and M. We observe that the network performance in terms of ASE improves by enabling CoMP. For instance, as the network shifts from a non-CoMP mode to a CoMP enabled UCRAN (i.e. from $M = 1$ to $M = 2$), we observe approximately 8% increase in ASE. This is mainly because if the closest UE-DBS link within an S-zone is affected by a blockage, there is a very low probability that the second closest UE-DBS link will also be affected by a blockage, thus ensuring the service reliability constraints at a typical UE. Besides, the dual-slope path loss model ensures that most of the interference dies out beyond the S-zone region. These two notions in parallel provide improvement in the ASE of the system with the enabling of CoMP.

An interesting observation is the consistency of area spectral efficiency values for any value of $M > 1$. There is an almost unnoticeable improvement when M is increased from beyond 2 as also noticed in [38]. This is mainly linked with the blockage probability considered in the network. In an environment, where it is highly probable that 2 or more serving DBSs can be simultaneously affected by blockages, we may be able to observe a noticeable increase in the ASE with an increase in M beyond 2. The change in the area spectral efficiency values concerning DBS density is due to the reasons discussed in Section VI (D). Since $M = 1$ reflects the scenario of UCRAN with single DBS activation, the result in Fig. 10 (a) shows that when random blocking is considered, the CoMP-based UCRAN with multiple DBS activations within an S-zone outperforms our earlier work [10], [29].

The performance in terms of area energy efficiency (AEE), which is defined as the ratio of area spectral efficiency and power consumption, is shown in Fig. 10 (b) for different values of DBS density and M. Intuitively, by enabling CoMP, the AEE should decrease because of higher power consumption by the activated DBSs. The results reveal that AEE decreases as more DBSs are enabled for cooperation. However, due to the dependence of AEE on ASE, the major drop in AEE occurs when M is increased from 1 to 2. The decrease in AEE values when M is changed from 1 to 2 is approximately 3.5%, whereas the increase in ASE is approximately 8%. Therefore, there is a visible trade-off between ASE and AEE values based on the number of cooperative DBSs that the network operators can utilize to design the network based on the service requirements of the users.

VII. Conclusion

In this work, we provided an analytical and numerical analysis on the impact of enabling CoMP in a UCRAN architecture. Contrary to the existing literature on analytical models of CoMP in UCRAN, we derived closed-form analytical expressions for activated data base station density, aggregate interference, coverage probability, area spectral efficiency, and energy efficiency. For CoMP, we presented a comparative analysis of three joint DBS transmission methods via cooperative DBSs in a user-centered virtual cell or an S-zone. Through our analysis which was supported by extensive Monte Carlo simulations, we showed that employing CoMP in a UCRAN architecture, with non-overlapping S-zones that uses spatial diversity for DBS activation with no blockages in the wireless communication channel, not only reduces the energy efficiency of the network but also degrades the coverage probability at a typical UE and consequentially the network-wide area spectral efficiency. However, we also discussed scenarios, in

particular highly blockage sensitive propagation, where the proposed design offered an improved area spectral efficiency. The analysis presented in this work provides a baseline on the design and planning of futuristic UCRAN based cellular networks.

We also investigated the impact of new degrees of freedom such as S-zone size and density of data base stations on the mean serviced UEs, area spectral efficiency, and energy efficiency of the network. The numerical results based on the derived analytical model revealed an interesting interplay between S-zone size and the density of data base stations. It is observed that for any number of cooperative data base stations in an S-zone, there exists an optimal size of S-zone and DBS density that maximizes the area spectral efficiency, and energy efficiency. However, the values of optimal S-zone size and data base station density that maximizes area spectral efficiency are quite different from the values that maximize network-wide energy efficiency. Therefore, there is a need for an AI-assisted self-organizing framework that is capable of dynamically orchestrating these network design parameters to offer the ideal tradeoff between these KPIs for a network operator.

The UCRAN architecture offers flexibility to schedule a cluster of users instead of a single user in an S-Zone. Serving multiple users in an S-Zone is particularly important when the UEs are more intensive than DBSs and a DBS can serve multiple UEs. The overlapped S-zones in this scenario will cause high-level interference to UEs in overlapped S-zone region. The research challenge here lies in designing clustering algorithms given the objective of scheduling more UEs in each transmission time interval, reducing interference, and reducing the need of switching ON/OFF DBSs in subsequent transmission time intervals resulting in improved energy efficiency. To further mitigate dominant interference, CoMP methods such as dynamic point selection and coordinated scheduling will be investigated in future work along with the clustering algorithms of UEs.

Appendix A

Proof of Theorem 1: The activation probability is computed based on the criterion that no more than M DBSs are activated in an S-zone iff: (i) there is a scheduled UE within a distance R_{szone} to at least 1 DBS, and (ii) no other DBS in an S-zone can provide superior channel gains to a scheduled user. Since both the constraints are independent events, we can compute p_{ACT} as:

$$p_{ACT} = Pr\Big(\Pi'_{UE} \cap b(\mathbf{d}, R_{szone}) \neq \phi \Big| \mathbf{d} \in \Pi'_{DBS}\Big) \cdot Pr\Big(\max\{ h_{d_1} r_{d_1}^{-\alpha}, ..., h_{d_M} r_{d_M}^{-\alpha}\}, 1 \leq m \leq \infty \Big| \mathbf{d} \in \Pi'_{DBS}, M < X\Big). \quad (21)$$

Solving in parts for each constraint separately, such that, $p_{ACT} = p'_{ACT} \cdot p''_{ACT}$, where

$$p'_{ACT} = Pr\Big(\Pi'_{UE} \cap b(\mathbf{d}, R_{szone}) \neq \phi \Big| \mathbf{d} \in \Pi'_{DBS}\Big) = 1 - \exp(-\lambda'_{UE} \pi R^2_{szone}), \quad (22)$$

and

$$p''_{ACT} = Pr\Big(\max\{h_{d_1} r_{d_1}^{-\alpha}, ..., h_{d_M} r_{d_M}^{-\alpha}\}, 1 \leq m \leq \infty \Big| \mathbf{d} \in \Pi'_{DBS}, M < X\Big), \quad (23)$$

where m is the actual number of DBSs in an S-zone which are distributed through the Poisson point process. The joint probability given above can be divided into two parts, that is, the probability that the actual number of DBSs in an S-zone is less than/equal to M or greater than M. Also, we assume that M is chosen such that $M < \lambda_{DBS} \pi R^2_{szone}$ where M can only be an integer number. Therefore,

$$p''_{ACT} = Pr\Big(\max\{h_{d_1} r_{d_1}^{-\alpha}, ..., h_{d_M} r_{d_M}^{-\alpha}\}, 1 \leq m \leq M \Big| \mathbf{d} \in \Pi'_{DBS}, M < X\Big) + Pr\Big(\max\{h_{d_1} r_{d_1}^{-\alpha}, ..., h_{d_M} r_{d_M}^{-\alpha}\}, M+1 \leq m \leq \infty \Big| \mathbf{d} \in \Pi'_{DBS}, M < X\Big). \quad (24)$$

Employing the conditional probability formula, we obtain:

$$p''_{ACT} = Pr(1 \leq m \leq M)\, Pr\Big(\max\{h_{d_1} r_{d_1}^{-\alpha}, ..., h_{d_M} r_{d_M}^{-\alpha}\} \Big| \mathbf{d} \in \Pi'_{DBS}, M < X, 1 \leq m \leq M\Big) + Pr(M+1 \leq m \leq \infty) Pr\Big(\max \{h_{d_1} r_{d_1}^{-\alpha}, ..., h_{d_M} r_{d_M}^{-\alpha}\} \Big| \mathbf{d} \in \Pi'_{DBS}, M < X, M+1 \leq m \leq \infty\Big). \quad (25)$$

If there are less than or equal to M DBSs in an S-zone then the probability of selection will be exactly 1 and if there are more than M DBS in an S-zone then only M out of m DBSs with the strongest channel gains will be selected. Therefore, the above expression can be rewritten as:

$$p''_{ACT} = \sum_{m=1}^{M} \exp(-X) \frac{(X)^m}{m!} \Big(1\Big) + \sum_{m=M+1}^{\infty} \exp(-X) \frac{(X)^m}{m!} \Big(\frac{M}{m}\Big). \quad (26)$$

After numerical simplification of the above expressions, we get:

$$p''_{ACT} = \frac{\Gamma(M+1, X)}{\gamma(M+1)} + \exp(-X) \left[\frac{M(X)^{M+1} {}_2F_2(1, M+1; M+2, M+2; X)}{(M+1)\gamma(M+2)} - 1 \right]. \quad (27)$$

Therefore, the modified density of activated DBSs can be approximated as:

$$p''_{ACT} = \Big(1 - \exp(-\lambda'_{UE} \pi R^2_{szone})\Big) \cdot \left(\frac{\Gamma(M+1, X)}{\gamma(M+1)} + \exp(-X) \left[\frac{M(X)^{M+1}}{} \frac{{}_2F_2(1, M+1; M+2, M+2; X)}{(M+1)\gamma(M+2)} - 1 \right] \right). \quad (28)$$

Appendix B

Proof of Theorem 2: The typical user is served successfully by a DBS only if the received SIR is greater than the desired threshold. Using the concepts of thinned marked Poisson processes [20] we derive the relationship between

the void probability of modified active DBSs (Π'_{DBS}) and $Pr(S < \gamma_{th} I)$.

$$P_r\Big(S < \gamma_{th} I\Big) = P_r(\Pi'_{DBS} = \emptyset) = \exp(-\Lambda(B)), \tag{29}$$

where the average measure $\Lambda(B)$ can be evaluated by:

$$\Lambda(B) = \int_0^{\infty} \int_B \lambda(r,h) dh dr, \tag{30}$$

where B is the area of ball region and $\lambda(r,h)$ is the intensity of the modified process which is given as [20]:

$$\lambda(r,h) = 2\pi\lambda_{DBS} r \mathbb{1}(hr^{-\alpha} \geq \gamma_{th} I) f_H(h). \tag{31}$$

Therefore,

$$\begin{aligned}\Lambda(B) &= \int_0^{\infty} \int_B 2\pi\lambda_{DBS} r \mathbb{1}(hr^{-\alpha} \geq \gamma_{th} I) f_H(h) dh dr \\ &= 2\pi\lambda_{DBS} \int_0^{R_{szone}} r \int_0^{\infty} \mathbb{1}(h \geq \gamma_{th} I r^{\alpha}) f_H(h) dh dr \\ &\overset{(a)}{=} 2\pi\lambda_{DBS} \int_0^{R_{szone}} r P_r(h \geq \gamma_{th} I r^{\alpha}) dr \\ &\overset{(b)}{=} \frac{\pi\lambda_{DBS}\delta\gamma(\delta, \gamma_{th} I R_{szone}^{\alpha})}{\gamma_{th}^{\delta} I^{\delta}},\end{aligned} \tag{32}$$

where (a) is due to the cumulative distribution function of an exponentially distributed random function, and (b) is obtained by defining the integration variable $t = \gamma_{th} I r^{\alpha}$ and integrating over t.

Substituting the value of Eq. (29) and Eq. (32) in Eq. (11), we obtain:

$$P_{cov}(\gamma_{th}, R_{szone}) = 1 - \mathbb{E}_{\mathbf{I}}\Big[exp\Big(-\frac{\pi\lambda_{DBS}\delta\gamma(\delta, \gamma_{th} I R_{szone}^{\alpha})}{\gamma_{th}^{\delta} I^{\delta}}\Big)\Big]. \tag{33}$$

Applying Jensen's inequality will give the lower bound for coverage probability as follows:

$$P_{cov}(\gamma_{th}, R_{szone}) \geq 1 - exp\Big(-\frac{\lambda_{DBS}\pi\delta\gamma(\delta, \gamma_{th}\mathbb{E}_{\mathbf{I}}[I] R_{szone}^{\alpha})}{\gamma_{th}^{\delta}\mathbb{E}_{\mathbf{I}}[I]^{\delta}}\Big). \tag{34}$$

Employing the value of $\mathbb{E}_{\mathbf{I}}[I]$ from Eq. (7) in the above expression concludes the proof.

ACKNOWLEDGEMENTS

This work is supported by the National Science Foundation under Grant Numbers 1923669, and 1730650. For more inquiries about these projects please visit www.AI4networks.com.

REFERENCES

[1] S. Sun, K. Adachi, P. H. Tan, Y. Zhou, J. Joung, and C. K. Ho, "Heterogeneous network: An evolutionary path to 5G," in *2015 21st Asia-Pacific Conference on Communications (APCC)*. IEEE, 2015, pp. 174–178.

[2] E. J. Oughton, Z. Frias, S. van der Gaast, and R. van der Berg, "Assessing the capacity, coverage and cost of 5G infrastructure strategies: Analysis of the Netherlands," *Telematics and Informatics*, vol. 37, pp. 50–69, 2019.

[3] M. U. B. Farooq, M. Qadir, and A. Imran, "Utilizing Loss Tolerance and Bandwidth Expansion for Energy Efficient User Association in HetNets," in *2020 IEEE 31st Annual International Symposium on Personal, Indoor and Mobile Radio Communications*. IEEE, pp. 1–6.

[4] A. Checko, H. L. Christiansen, Y. Yan, L. Scolari, G. Kardaras, M. S. Berger, and L. Dittmann, "Cloud RAN for mobile networks—A technology overview," *IEEE Communications surveys & tutorials*, vol. 17, no. 1, pp. 405–426, 2014.

[5] U. S. Hashmi, A. Islam, K. M. Nasr, and A. Imran, "Towards User QoE-Centric Elastic Cellular Networks: A Game Theoretic Framework for Optimizing Throughput and Energy Efficiency," in *2018 IEEE 29th Annual International Symposium on Personal, Indoor and Mobile Radio Communications (PIMRC)*, Sep. 2018, pp. 1–7.

[6] S. Bassoy, H. Farooq, M. A. Imran, and A. Imran, "Coordinated Multi-Point Clustering Schemes: A Survey," *IEEE Communications Surveys and Tutorials*, vol. 19, no. 2, pp. 743–764, 2017.

[7] S. Chen, T. Zhao, H. H. Chen, Z. Lu, and W. Meng, "Performance analysis of downlink coordinated multipoint joint transmission in ultra-dense networks," *IEEE Network*, vol. 31, no. 5, pp. 106–114, 2017.

[8] Y. Zhang and Y. J. Zhang, "User-centric virtual cell design for Cloud Radio Access Networks," *IEEE Workshop on Signal Processing Advances in Wireless Communications, SPAWC*, vol. 2014-Octob, no. October, pp. 249–253, 2014.

[9] J. Shi, C. Pan, W. Zhang, and M. Chen, "Performance analysis for user-centric dense networks with mmwave," *IEEE Access*, vol. 7, pp. 14 537–14 548, 2019.

[10] U. S. Hashmi, S. A. R. Zaidi, A. Imran, and A. Abu-Dayya, "Enhancing Downlink QoS and Energy Efficiency Through a User-Centric Stienen Cell Architecture for mmWave Networks," *IEEE Transactions on Green Communications and Networking*, vol. 4, no. 2, pp. 387–403, 2020.

[11] Q. Wang, D. Jiang, J. Jin, G. Liu, Z. Yan, and D. Yang, "Application of BBU+ RRU based CoMP system to LTE-Advanced," in *2009 IEEE International Conference on Communications Workshops*. IEEE, 2009, pp. 1–5.

[12] M. Nabeel and F. Dressler, "Experimental evaluation of receive diversity techniques in distributed sensor networks," *Ad Hoc Networks*, vol. 99, p. 102066, 2020.

[13] N. Guo, M.-L. Jin, and N. Deng, "Coverage analysis for heterogeneous network with user-centric cooperation," *IEEE Systems Journal*, vol. 13, no. 3, pp. 2724–2727, 2018.

[14] J. Shi, H. Xu, Z. Yang, and M. Chen, "Energy efficient beamforming for user-centric virtual cell networks," *IEEE Transactions on Green Communications and Networking*, vol. 3, no. 3, pp. 575–590, 2019.

[15] S. Zaidi, O. B. Smida, S. Affes, U. Vilaipornsawai, L. Zhang, and P. Zhu, "User-centric base-station wireless access virtualization for future 5g networks," *IEEE Transactions on Communications*, vol. 67, no. 7, pp. 5190–5202, 2019.

[16] M. Elhattab, M.-A. Arfaoui, and C. Assi, "Comp transmission in downlink noma-based heterogeneous cloud radio access networks," *IEEE Transactions on Communications*, vol. 68, no. 12, pp. 7779–7794, 2020.

[17] M. Di Renzo, A. Zappone, T. T. Lam, and M. Debbah, "System-level modeling and optimization of the energy efficiency in cellular networks—a stochastic geometry framework," *IEEE Transactions on Wireless Communications*, vol. 17, no. 4, pp. 2539–2556, 2018.

[18] G. T. 36.819, "Coordinated Multi-Point Operation for LTE Physical Layer Aspects," 2013.

[19] S. Andreev, V. Petrov, M. Dohler, and H. Yanikomeroglu, "Future of ultra-dense networks beyond 5G: Harnessing heterogeneous moving cells," *IEEE Communications Magazine*, vol. 57, no. 6, pp. 86–92, 2019.

[20] S. N. Chiu, D. Stoyan, W. S. Kendall, and J. Mecke, *Stochastic geometry and its applications*. John Wiley & Sons, 2013.

[21] A. Imran, M. A. Imran, A. Abu-Dayya, and R. Tafazolli, "Self organization of tilts in relay enhanced networks: A distributed solution," *IEEE Transactions on Wireless Communications*, vol. 13, no. 2, pp. 764–779, 2014.

[22] M. Haenggi, "Mean interference in hard-core wireless networks," *IEEE Communications Letters*, vol. 15, no. 8, pp. 792–794, 2011.

[23] Q. Cui, X. Yu, Y. Wang, and M. Haenggi, "The SIR meta distribution in poisson cellular networks with base station cooperation," *IEEE Transactions on Communications*, vol. 66, no. 3, pp. 1234–1249, 2018.

[24] W. Sun and J. Liu, "2-to-M Coordinated Multipoint-Based Uplink Transmission in Ultra-Dense Cellular Networks," *IEEE Transactions on Wireless Communications*, vol. 17, no. 12, pp. 8342–8356, 2018.

[25] S. Chen, F. Qin, B. Hu, X. Li, and Z. Chen, "User-centric ultra-dense networks for 5G: challenges, methodologies, and directions," *IEEE Wireless Communications*, vol. 23, no. 2, pp. 78–85, 2016.

[26] A. AlAmmouri, J. G. Andrews, and F. Baccelli, "SINR and throughput of dense cellular networks with stretched exponential path loss," *IEEE Transactions on Wireless Communications*, vol. 17, no. 2, pp. 1147–1160, 2017.

[27] A. Taufique, M. Jaber, A. Imran, Z. Dawy, and E. Yacoub, "Planning wireless cellular networks of future: Outlook, challenges and opportunities," *IEEE Access*, vol. 5, pp. 4821–4845, 2017.

[28] M. Alonzo, S. Buzzi, A. Zappone, and C. D'Elia, "Energy-efficient power control in cell-free and user-centric massive mimo at millimeter wave," *IEEE Transactions on Green Communications and Networking*, vol. 3, no. 3, pp. 651–663, 2019.

[29] Hashmi, Umair Sajid and Zaidi, Syed Ali Raza and Imran, Ali, "User-Centric Cloud RAN: An Analytical Framework for Optimizing Area Spectral and Energy Efficiency," *IEEE Access*, vol. 6, pp. 19 859–19 875, 2018.

[30] G. Auer, V. Giannini, C. Desset, I. Godor, P. Skillermark, M. Olsson, M. A. Imran, D. Sabella, M. J. Gonzalez, O. Blume *et al.*, "How much energy is needed to run a wireless network?" *IEEE Wireless Communications*, vol. 18, no. 5, pp. 40–49, 2011.

[31] R. Gupta, E. C. Strinati, and D. Kténas, "Energy efficient joint DTX and MIMO in cloud radio access networks," in *2012 IEEE 1st International Conference on Cloud Networking (CLOUDNET)*. IEEE, 2012, pp. 191–196.

[32] A. J. Fehske, P. Marsch, and G. P. Fettweis, "Bit per joule efficiency of cooperating base stations in cellular networks," *2010 IEEE Globecom Workshops, GC'10*, pp. 1406–1411, 2010.

[33] H. S. Lichte, S. Valentin, and H. Karl, "Expected interference in wireless networks with geometric path loss: a closed-form approximation," *IEEE communications letters*, vol. 14, no. 2, pp. 130–132, 2010.

[34] H. P. Keeler, B. Błaszczyszyn, and M. K. Karray, "SINR-based k-coverage probability in cellular networks with arbitrary shadowing," in *2013 IEEE International Symposium on Information Theory*. IEEE, 2013, pp. 1167–1171.

[35] Y. Yang, K. W. Sung, J. Park, S.-L. Kim, and K. S. Kim, "Cooperative transmissions in ultra-dense networks under a bounded dual-slope path loss model," in *2017 European Conference on Networks and Communications (EuCNC)*. IEEE, 2017, pp. 1–6.

[36] P. Korrai and D. Sen, "Downlink SINR coverage and rate analysis with dual slope pathloss model in mmWave networks," in *2017 IEEE Wireless Communications and Networking Conference (WCNC)*. IEEE, 2017, pp. 1–6.

[37] C. Galiotto, N. K. Pratas, N. Marchetti, and L. Doyle, "A stochastic geometry framework for LOS/NLOS propagation in dense small cell networks," in *2015 IEEE International Conference on Communications (ICC)*. IEEE, 2015, pp. 2851–2856.

[38] M. Nabeel, V. K. Singh, and F. Dressler, "Efficient Data Gathering for Decentralized Diversity Combining in Heterogeneous Sensor Networks," in *2019 IEEE Wireless Communications and Networking Conference (WCNC)*. IEEE, 2019, pp. 1–6.